A comparison study of the adsorption of metal ions by chitosan derivatives in aqueous solution

E. Igberase*, P.O. Osifo

Department of Chemical Engineering, Vaal University of Technology, Private Mail Bag X021, Vanderbijlpark 1900, South Africa, Tel. +27 84 949 8111, email: ephraimiberase@gmail.com (E. Igberase)

ABSTRACT

In this investigation, three chemicals were identified as grafting materials and used separately for the grafting of the cross-linked beads in an attempt to determine which of the beads will be the most efficient material in adsorption studies. On this note, chitosan beads were formed, and the beads were cross-linked with glutaraldehyde, the cross-linked beads were thereafter separated with ethylene acrylic acid, 4-aminobenzoic acid, and ethylenediaminetetraacetic acid to produce $GXCS_1$, $GXCS_2$, and $GXCS_3$, respectively. The chemical functionalities of the beads were obtained by Fourier-transform infrared spectroscopy and scanning electron microscope. Adsorption of Pb(II), Cu(II), Ni(II), Zn(II), Cr(VI), and Cd(II) ions from single component aqueous mixture by the three sets of developed adsorbents was examined separately in batch mode as a function of pH, initial concentration, adsorbent dose, contact time, stirring speed and ionic strength. A pH model was applied to fit equilibrium data obtained from the adsorption experiment; the model takes into consideration the influence of pH. The amine concentration of chitosan beads (CS) and cross-linked chitosan beads (XCS) was found to be 3.9 and 3.2 mmol/g, respectively. The maximum adsorption capacity (q_{max}) was observed to be 5.73 mmol/g for $GXCS_1$, 5.21 mmol/g for $GXCS_2$ and 4.61 mmol/g for $GXCS_3$. Kinetics was better explained by pseudo-second-order and intra-particle model with correlation a coefficient (R^2) in the range of 0.93 to 1.00. Regeneration of the used adsorbents was effective, and the adsorbents could be re-applied in adsorption studies without any significant loss in maximum adsorption capacity (q_{max}).

Keywords: Adsorption; pH model; Maximum adsorption capacity; Kinetic; Desorption.

1. Introduction

Due to pressing universal health hazards emanating from heavy metal ion contamination and its diffusion into our food chain via the pollution of a watercourse, rigid guidelines have been approved by the United States Environmental Protection Agency (USEPA) for heavy metal loaded wastewater discharge [1,2]. Heavy metals such as Pb(II), Cu(II), Ni(II), Zn(II), Cr(VI) and Cd(II) are a collection of metals with an atomic density greater than 6.0 g/cm³, some heavy metals are important but high concentration may signify severe danger to human health and the ecological system [1]. The major source of these metal ions is the increasing industrialization and urbanization, which results in the global use of these metal ions. These industries include chemical, electroplating, leather, tannery, galvanizing, mining, pharmaceutical, pigment and dye industries [3–5]. Among the dangers, these heavy metals are known to cause human health problems including lung and kidney problems, pulmonary fibrosis, circulatory collapse, intravascular hemolysis, renal failure, nephritis, fever, vertigo, diarrhea, vomiting epigastric pain, nausea, intense gastrointestinal irritation, acute multisystem organ failure, coma and even death [6].

* Corresponding author.

Different approaches have been applied over the years for the removal of metal ions but these techniques, including chemical precipitation, membrane separation, ion exchange, and electrolysis, have shown to be inefficient due to high operational cost and low removal of metal ions [7–9] The hunt for efficient, low-cost, readily available, sludge-free, profitable, effortless and cleaner technology operation has led to the development and utilization of adsorption process [10]. Up to date, chitosan is useful as an adsorptive material due to its market availability, large surface area, high adsorption capacity, simple processing, nontoxicity, being environmentally friendly and its regeneration capability after adsorption [11,12]. Chitosan is a derivative of the N-deacetylation of chitin, which is a naturally occurring polysaccharide found in crustacean and microbial biomass. The presence of amine (–NH$_2$) and hydroxyl functional group gives the adsorbent its unique adsorption qualities. However, chitosan has its drawbacks, which reduces its usage; hence, current studies have focused on modification methods. The physical modification includes converting chitosan powder or flakes into gel beads for easy handling and easier diffusion to binding sites, while chemical modification includes cross-linking and grafting. Modification of chitosan by cross-linking makes chitosan beads insoluble in acid solution, thereby increasing its mechanical and chemical stability. This method has shown to have reduced adsorption capacity as the amine group of chitosan is involved in the cross-linking process, hence grafting of some chemical material onto the backbone of the cross-linked chitosan beads becomes important.

In this work, studies on the uptake efficiencies of heavy metal ions from synthetic solutions were studied with modified chitosan beads. The modification process includes cross-linking with glutaraldehyde and grafting of the cross-linked beads separately with chemicals such as ethylene acrylic acid, 4-aminobenzoic acid, and ethylenediaminetetraacetic acid. The sets of beads were characterized by Fourier-transform infrared spectroscopy (FTIR) and scanning electron microscope (SEM). The effect of adsorption variables on the adsorption of metal ions onto the developed adsorbent was examined. The developed adsorbents were applied separately in the removal of Pb(II), Cu(II), Ni(II), Zn(II), Cr(VI) and Cd(II) in single component batch studies to determine the most favorable adsorbent.

2. Experiment section

2.1. Materials and equipment

All chemicals used in this investigation were of scientific quality and were applied without more treatment purification. Chitosan powder with a degree of deacetylation of 74 percent was acquired from China. Glutaraldehyde, ethylene acrylic acid, 4-aminobenzoic acid, and ethylenediaminetetraacetic acid were purchased from Sigma-Aldrich (South Africa). A domestic oven with a medium-low power was applied in the grafting of XCS at a contact time of 20 min. Hydrochloric acid, acetic acid, sodium hydroxide, sodium nitrate, and aluminum sulfate were obtained from Sigma-Aldrich (South Africa). The pH of the mixture was regulated with a pH meter and obtained from Sigma-Aldrich

(South Africa). Ultima 888 water distiller was applied in obtaining distilled water. A shaker was applied in adsorption studies to attain equilibrium.

2.2. Adsorbate preparation

The concentrated adsorbate solution of Pb(II), Cu(II), Ni(II), Zn(II), Cr(VI) and Cd(VI) was acquired by singly formulating 0.1 M of CuSO$_4$·5H$_2$O, CdCl$_2$·H$_2$O, Zn(NO$_3$)$_2$·6H$_2$O, Pb(NO$_3$)$_2$, NiSO$_4$·6H$_2$O and K$_2$CrO$_7$. This concentrated adsorbate solution was also mixed with distilled water to achieve suitable initial concentrations.

2.3. Adsorbent preparation

Chitosan powder was used in formulating the beads. The solution of chitosan was produced by dissolving 30 g of chitosan powder in 1 L open neck flask containing a mixture of 950 mL distilled water and 50 mL acetic acid. The solution was passed via a pipette with the effort of a peristaltic pump to a one molar solution of sodium hydroxide, which resulted in the production of chitosan gel beads (CS). The gel beads were cleaned with distilled water multiple times to separate any residue of sodium hydroxide. The gel beads formed were mixed with a 2.5% glutaraldehyde solution and agitated with a magnetic stirrer for six hrs in order for a cross-linking reaction to take place. In obtaining the degree of cross-linking (DCL), a standard titration method put forward [13] and was used to determine the amine concentration and the DCL in the chitosan. Exactly 10.000 g of the cross-linked beads were weighed in a 30 mL glass tube. A 100 mL suspension was prepared using distilled water and the suspension was continuously stirred with a magnetic stirrer during titration with a 1.000 M HCl solution. The pH of the solution was recorded after set time intervals. The data obtained from the titration results were used to determine the amine concentration and the DCL was calculated using Eq. (1).

$$DCL = \frac{\left[-NH_2\right] - \left[-NH_2\right]_T}{\left[-NH_2\right]} \tag{1}$$

in which [–NH$_2$] and [–NH$_2$]$_T$ are the amine concentration for non-cross-linked beads and cross-linked beads, respectively.

The XCS were once more cleansed with distilled water multiple times to remove any surplus glutaraldehyde. Finally, the XCS was grafted using the microwave technique with a medium-low power for 20 min. This was achieved by singly mixing 4 g of DCDS in 0.1 M of ethylene acrylic acid, 4-aminobenzoic acid, and ethylenediaminetetraacetic acid respectively in a flask. This flask was placed in a domestic microwave for grafting reaction to occur. The beads were again washed with distilled water and ready to be applied for further investigations.

2.4. Characterization of the beads

1.0 g of CS, (XCS), GXCS$_1$, GXCS$_2$, and GXCS$_3$ were weighed respectively and heated to dryness in an oven at a temperature of 60°C. The dried beads were then separately grounded until reaching powdered form. The infrared

quantification was carried out with a Shimadzu FTIR model 8300 Kyoto, Japan, and the spectrum was entered in the limit of 500–4,000 cm^{-1}. The SEM investigation was performed separately cutting the five sets of beads in order to get a striking view of the internal structure. The bisected beads were then covered with gold and the structure of the coated beads was examined with a JEOL 733 super probe from Kyoto Japan.

2.5. Adsorption studies

A fixed mass of the three different developed adsorbents was each moved into a series of Erlenmeyer flasks, then a small quantity (100 mL) of a given concentration was transferred into each of the flasks. The pH of the mixture was normalized using 0.1 M HCl/NaOH. The influence of operating variables was investigated at pH 2–8, initial concentration 0.5–2.5 mmol/L, adsorbent dosage 2–10 g/L, ionic strength 0.05–0.2 mmol/L and contact time 10–80 min. Equilibrium was performed by placing a given mass of adsorbent into a sequence of 250 mL Erlenmeyer flasks and the volume of each flask was set to 100 mL of adsorbate with different initial concentrations of 0.5, 1.0, 1.5, 2.0 and 2.5 mmol/L. The flasks were placed in a shaker and stirred for a given period of time. After equilibrium, an unclouded metal sample was taken and examined with an atomic absorption spectrophotometer to examine the amount of adsorbate adsorbed. The equilibrium binding capacity was estimated from the mass balance equation as shown in Eq. (2).

$$q_e = \frac{(C_0 - C_e) \times V}{M} \tag{2}$$

where q_e (mg/g) is the equilibrium adsorption capacity, C_0 and C_e is the initial and equilibrium concentration (mg/L) of adsorbate in solution respectively, while V (mL) is the volume and M (g) is the mass of the adsorbent. The removal efficiency was obtained using Eq. (3).

$$\%R = \frac{(C_0 - C_e)}{C_0} \times 100 \tag{3}$$

2.6. Kinetic experiment

A given mass of adsorbent was separately mixed with 100 mL of Pb(II), Cu(II), Ni(II), Zn(II), Cr(VI) and Cd(II) ions solution in a series of 250 mL Erlenmeyer flasks having an initial concentration of 0.5 mmol/L. This concentration was prepared separately from a concentrated adsorbate solution and then regulated to the required pH value. To attain an equilibrium, the flasks were placed in a shaker, the solutions were shaken at 120 rpm and the temperature adjusted to 45°C. 4 mL samples were taken at an interval of 20, 40 and 60 min and examined with an atomic absorption spectrophotometer for their adsorbate removal.

2.7. Desorption experiment

After adsorption, the grafted cross-linked beads loaded separately with Pb(II), Cu(II), Ni(II), Zn(II), Cr(VI) and Cd(II) ions were washed with distilled water before treating it with 50 mL of 0.5 M HCl and contact time of 180 min. The percentage of desorption was estimated using Eq. (4).

$$\%\text{desorption} = \frac{C_e}{C_0} \times 100 \tag{4}$$

where C_e represents the final metal ion concentration in the desorption medium and C_0 represents the initial concentration of the metal ion.

3. Theory of evaluation of data

3.1. pH-equilibrium model

This model is similar to the equilibrium model as given by [13] and is obtained from two equilibrium reactions and a nitrogen mass balance. Adsorption via coordination has been projected as the binding mechanism for chitosan as given in Eq. (5) and the equilibrium constant for this reaction is expressed in Eq. (6), with the chitosan binding sites expressed as –NH$_2$.

$$M_{(aq)}^{2+} + n(-NH_2) + mH_2O \rightleftharpoons$$
$$[M(-NH_2)_n, (OH^-)_m]^{(2-m)+} + mH^+ \tag{5}$$
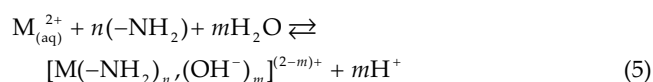
where n is the amount of amine group and m is the amount of hydroxide group.

If $[M(-NH)_{n'}$ (OH$^-$)]$^{(2-m)+}$ is described as [M*], the equivalent equilibrium constant is presented in Eq. (6):

$$K_{ads} = \frac{[M^*][H^+]^m}{[-NH_2][M_{aq}^{2+}]} \tag{6}$$

The reaction of chitosan can also occur according to:

$$-NH_2 + H^+ \rightleftharpoons -NH_3^+ \tag{7}$$

The acid-base constant for this reaction of Eq. (7) can be estimated using an experimental titration curve via titration experiment. From this experiment, the degree of protonation, α, expressed as the ratio of the protonated amine groups to the total amine groups that are not complexed with adsorbate, is derived as:

$$\alpha = \frac{[-NH_3^+]}{[-NH_2] + [-NH_3^+]} \tag{8}$$

The total amine group concentration is equal to the sum of the concentration of unbounded amine groups [–NH$_2$], the protonated amine groups [–NH$_3^+$] and the adsorbate spent amine groups ($n \cdot$[M*]):

$$[-NH_2]_T = [-HN_2] + [-NH_3^+] + n[M^*] \tag{9}$$

Combining Eqs. (8) and (9) gives:

$$\left[-NH_3^+\right] = \alpha\left(\left[-NH_2\right]_T - n\left[M^*\right]\right) \tag{10}$$

Substituting for $[R–NH_3^+]$ in Eq. (10) gives

$$\left[-NH_2\right] = \left(\left[-NH_2\right]_T - n\left[M^*\right]\right)(1-\alpha) \tag{11}$$

where $[M^*]$ is the quantity of adsorbate adsorbed by the adsorbent at equilibrium, which is commonly expressed as q_e.

If the amine sites are accessible for binding, then the total amine concentration has a correlation with the maximum capacity (q_{max}) and n, as shown in Eq. (12).

$$q_{max} = \frac{\left[-NH_2\right]_T}{n} \tag{12}$$

which yields Eq. (13)

$$\left[-NH_2\right] = n\left(\left(q_{max} - q_e\right)(1-\alpha)\right) \tag{13}$$

Substituting Eq. (13) into Eq. (6) gives:

$$K_{ads} = \frac{q_e\left[H^+\right]^m}{\left[n\left(\left(q_{max}-q_e\right)(1-\alpha)\right)\right]^n C_e} \tag{14}$$

Eq. (14) is expressed in quantifiable quantities that can be applied in evaluating the equilibrium constant. Taking the log of both sides of Eq. (14) gives Eq. (15).

$$\log\frac{q_e}{\left[n\left(\left(q_{max}-q_e\right)(1-\alpha)\right)\right]^n C_e} = \log K_{ads} - m\log\left[H^+\right] =$$

$$\log K_{ads} + m\text{pH} \tag{15}$$

q_e, C_e and α obtained from practical quantification, q_{max} can be fitted in the graph of the left-hand side of Eq. (15) against pH obtained at equilibrium. The value of n is selected for some distinct cases, usually between one and two. The value of K_{ads} is evaluated from the intercept of the linear plot on the y-axis and the slope of the plot is used to obtain m.

3.2. Adsorption kinetics

The assessment of system kinetics in adsorption studies can reveal the adsorption mechanism. Many authors apply the pseudo-first-order kinetics of Lagergren [2], the pseudo-second-order kinetic model that was presented by Ho and McKay [14] and the intra-particle diffusion model as described in Eqs. (16)–(18) to analyze kinetic data.

$$\log\left(q_e - q_t\right) = \log\left(q_e\right) - t\frac{K_1}{2.303} \tag{16}$$

where q_e and q_t shows the amount of adsorbate absorbed on the adsorbent (mmol/g) at equilibrium and time t, respectively.

K_1 (min^{-1}) is the rate constant of the pseudo-first-order kinetics. The value of the rate constant, K_1, can be estimated from the linear plot of $\log(q_e–q_t)$ against t.

$$\frac{t}{q_t} = \frac{1}{K_2 q_e^2} + \frac{1}{q_e}t \tag{17}$$

where K_2 (g/mmol min) is the rate constant for a pseudo-second-order model. The slope and intercept of the straight-line plot of t/q_t vs. t, provides the values of q_e and K_2, respectively.

The intra-particle diffusion model is of importance because it is the rate determining step in any liquid binding process [15]. In a well-agitated batch binding process, the intra-particle diffusion model can be used to examine the binding process occurring in the adsorbent [16]. Intra-particle diffusion model varies relatively with the rate constant and the square root of time.

$$q_t = K_{idm}\sqrt{t} \tag{18}$$

t is the time (min), K_{idm} (mmol/gmin$^{1/2}$) is the intra-particle diffusion rate constant. The slope of the straight-line plot of q_t vs. $t^{1/2}$ provides the value of K_{idm}.

4. Results and discussion

4.1. Characterisation

4.1.1. SEM result

SEM was employed to study the structure and transformation of chitosan after cross-linking and grafting. SEM micrographs of the separate set of beads are presented in Figs. 1a–e. The surface of XCS seems to be more level in contrast to CS, which may be due to the presence of glutaraldehyde on the backbone of CS. In Figs. 1c–e, the grafting of ethylene acrylic acid, 4-aminobenzoic acid and ethylenediaminetetraacetic acid respectively onto the backbone of XCS causes the surface of the adsorbent to be smooth.

4.1.2. FTIR result

To verify the functional groups is of paramount importance and to give a measurable change among the set of beads, the FTIR spectrum was applied. Fig. 2 describes the spectrum. CS comprises of several functional group properties of glycosidic substances. The plot of CS reveals the emerging attribute; broadband at 3,396 cm^{-1} showing the existence of exchangeable hydrogen ions, which originate from hydroxyl and amine group (Kampalanonwat and Supaphol [5]). In the aliphatic region, which is usually between 2,800–3,000 cm^{-1}, there is a peak at wavelength 2,847 cm^{-1} which corresponds to asymmetric –CH$_2$ stretching (Dong et al. [25]; Tirtom et al. [17]). The spectrum exhibited a major peak at 1,000 cm^{-1} which is attributed to C–O stretching vibrations, it originates from aliphatic ethers and alcohols and signifies oxygen-enriched functional groups [17]. The peak at wavelength 1,512 cm^{-1} is assigned to N=O stretching vibration. The peak at 1,817 cm^{-1} is ascribed to C=O stretching vibrations of ketone and amide. The peak at 779 cm^{-1} is related to

aromatic out-of-plane C–H deformations. The peaks at 2,159 and 2,159 cm^{-1} are attributed to C≡C stretching vibrations of an alkyl group.

When CS was cross-linked with glutaraldehyde, the difference was obvious, suggesting that cross-linking modified the properties of CS. The specific differences that were observed comprise of left shift in the band, which is from 3,396 to 3,463 cm^{-1}, left shift in the peak, which is from 2,847 to 2,840 cm^{-1}, left shift in the peak, which is from 1,734 to 1,650 cm^{-1} and right shift in the peak, which is from 1,000 to 1,020 cm^{-1}. The repositing in the peaks is due to the successful cross-linking reaction between glutaraldehyde and CS. The sharp peaks at a wavelength 1,217 and 1,508 cm^{-1} correspond to C–N and N=O stretching vibration, respectively. IR spectra showed an increase in intensity between wavelength 1,217 and 1,653 cm^{-1}.

FTIR analysis results showed a change in characteristics for grafted beads compared to the cross-linked beads. For GXCS$_1$, the properties include repositioning of peaks, the formation of new peaks and extended intensity. The repositioned peaks include left shift from 3,463 to 3,339 cm^{-1}, right shift from 2,840 to 2,844 cm^{-1} and right shift from 1,650 to 1,664 cm^{-1}. The new peak at 1,577 cm^{-1} corresponds to N–H medium bending vibrations. The GXCS$_1$ revealed a rise in intensity between 1,390 and 1,617 cm^{-1}.

For the GXCS$_2$, the repositioned peaks comprise of left shift from 3,463 to 3389 cm^{-1}, right shift from 2,840 to 2,875 cm^{-1} and left shift from 1,650 to 1,659 cm^{-1}. The spectrum revealed an increase in intensity between 920 cm^{-1} and 1352 cm^{-1}. This presents the affirmation of grafting.

For the GXCS$_3$ beads, the repositioning of peaks comprises of left shift from 3,463 to 3,386 cm^{-1}, right shift from 2,840 to 2,950 cm^{-1} and right shift from 1,650 to 1,662 cm^{-1}. The spectrum exhibited a rise in intensity between 1,320 to 1,616 cm^{-1}. Grafting of EDTA onto XCS is again verified by more peaks at 705 and 853 cm^{-1}, which correlates to C–H bending vibration.

4.2. Single component adsorption variables

4.2.1. Effect of pH

pH is directly associated with metal ions and adsorbent functional groups and plays a major part in the binding of metal ions. It also impacts on the degree of ionization and surface characteristics of adsorbents [18,19]. Figs. 3–c elucidate the influence pH has on the binding of metal ions by the three different sets of developed adsorbents at pH values of 2–8. It was observed in Fig. 3 that at a pH of 2 the removal efficiency was higher than 50%. Which may be due to the
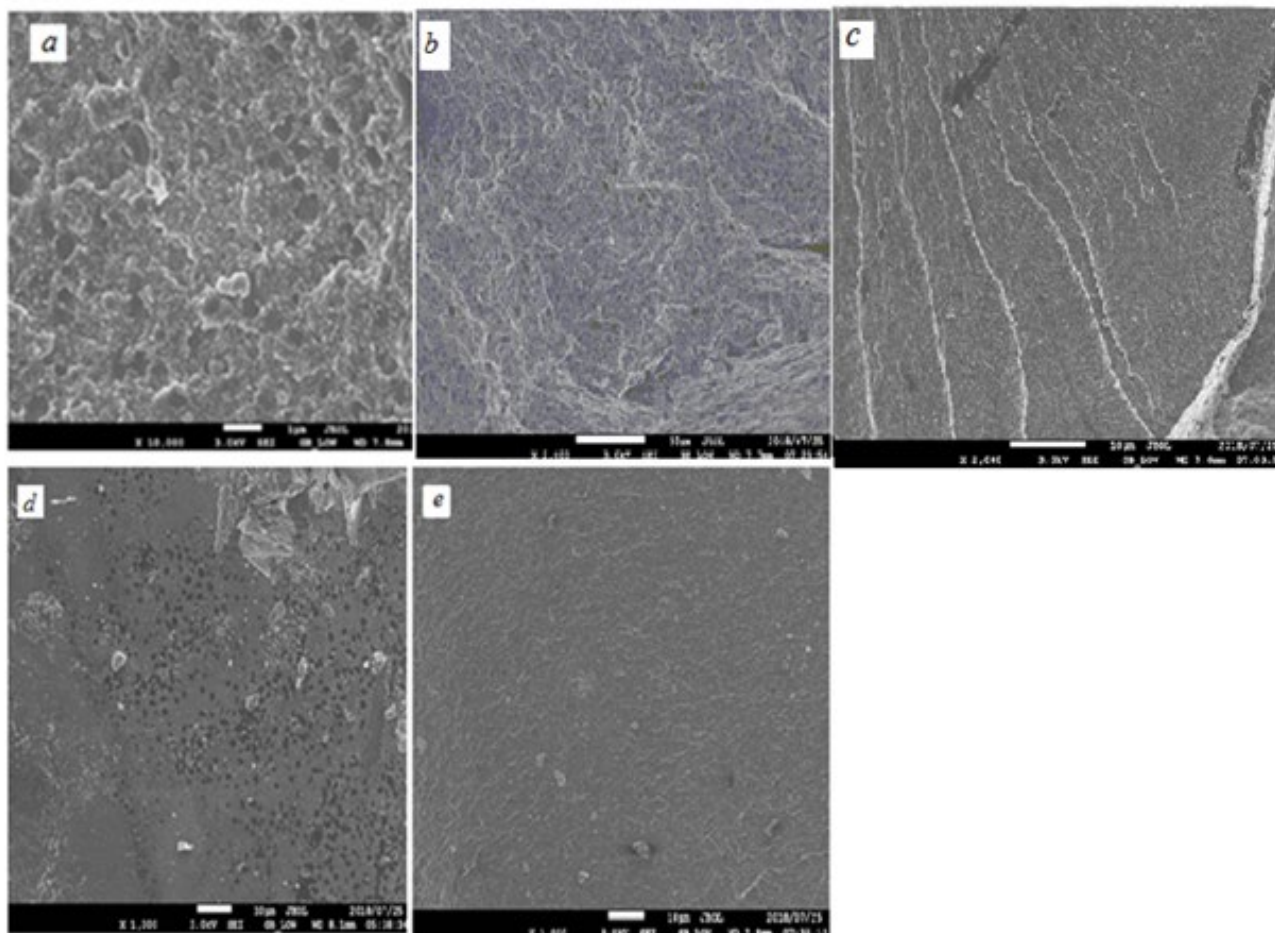

Fig. 1. SEM analysis of (a) CS, (b) XCS, (c) GXCS$_1$, (d) GXCS$_2$, and (e) GXCS$_3$, respectively.

Fig. 2. FTIR of CS, XCS, GXCS$_1$, GXCS$_2$, and GXCS$_3$, respectively.

reaction of XCS and carboxylic functional group. pH values obtained at maximum removal efficiency were 5, 5, 7, 6, 6 and 6 for Pb(II), Cu(II), Ni(II), Zn(II) Cd(II) and Cr(VI) respectively. Better efficiencies at these pH values may be due to the presence of an unbound lone pair of electrons on nitrogen atoms, which is important for bonding with adsorbate and to deliver the required adsorbate/adsorbent complex [20]. Also,

at low pH, the adsorbent is occupied with protons, which can prevent the binding of adsorbate owing to the competition for adsorption sites resulting in lower removal efficiency. With rising pH, the repelling force that is present between the adsorbate in the mixture and the functional groups in the adsorbent decreases, thus increasing the removal of metal ions in solution, at pH exceeding the maximum value indissoluble adsorbate hydroxide starts to precipitate from the mixture, which causes a reduction in the binding of adsorbate onto adsorbent in the mixture. The influence of pH can also be elucidated in relation to the point of zero charge (pH$_{PZC}$) of the adsorbent. pH$_{PZC}$ is the point where the surface acidic or basic functional group no longer contributes to the pH of the solution [21]. However, the surface of the adsorbent is negatively charged at pH > pH$_{PZC}$, positively charged at pH < pH$_{PZC}$ and neutral at pH = pH$_{PZC}$. The pH$_{PZC}$ of GXCS$_1$, GXCS$_2$, and GXCS$_3$ was 3.8, 4.5, and 4.4, respectively, which is ideal for binding studies since the adsorbent surface is negatively charged.

4.2.2. Effect of contact time

Figs. 4a–c describe the influence of contact time on the binding of metal ions at the contact time limit of 10–80 min by GXCS$_1$, GXCS$_2$, and GXCS$_3$ respectively. It was noticed that 40 min was sufficient to establish equilibrium for the

Fig. 3. Influence of pH on percentage removal of adsorbate by (a) GXCS$_1$, (b) GXCS$_2$, and (c) GXCS$_3$, respectively (Conditions: contact time: 70 min, temperature: 25°C, initial concentration: 0.8 mmol/L, and agitation speed: 120 rpm).
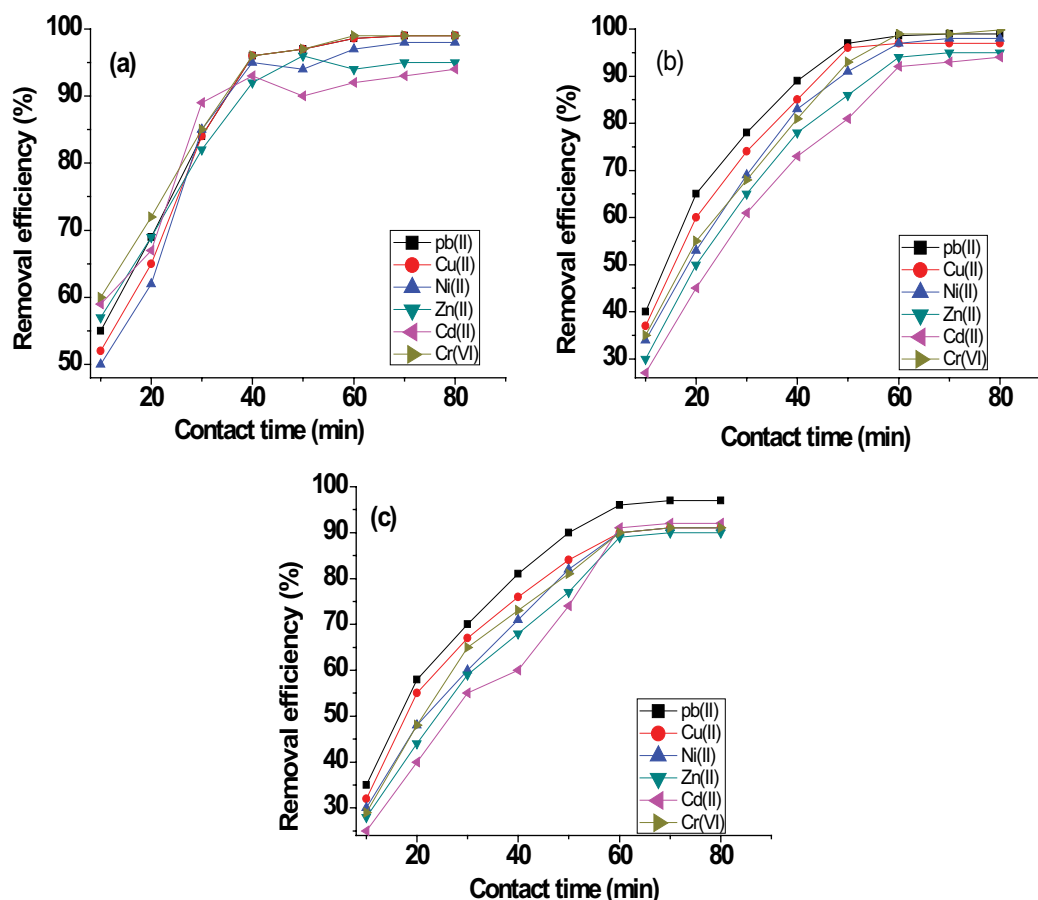
Fig. 4. Influence of contact time on percentage removal of adsorbate by (a) GXCS$_1$, (b) GXCS$_2$, and (c) GXCS$_3$, respectively (Conditions: pH: Pb^{2+}(5), Cd^{2+}(6), Zn^{2+}(6), Ni^{2+}(7), Cu^{2+}(5), and Cr^{6+}(6), temperature: 25°C, initial concentration: 0.8 mmol/L, and agitation speed: 120 rpm).

binding of metal ions onto GXCS$_1$. In the case of GXCS$_2$, it was observed that 45 min was sufficient to establish equilibrium for Pb(II), Cu(II) and Ni(II) while it took 55 min for Zn(II) and Cd(II). Also, for GXCS$_3$, it took 60 min to reach equilibrium for all metal ions. The adsorption was very fast at the initial stage for all metal ions adsorption onto the three sets of beads, due to a sufficient and properly-aligned site available for the binding of adsorbate and began to be slow pending the establishment of equilibrium. However, the binding sites are enclosed with adsorbate, which resulted in repulsion with time rise. A similar result was achieved by [22], the researchers investigated the influence of contact time on the binding of Pb(II), Cd(II) and Ni(II) on activated bentonite at the contact time of 1–60 min. The result showed that 40 min was enough to reach equilibrium time and the workers reported a large number of available sites as the reason for fast adsorption. In another study by [23], the influence of contact time was examined on the binding of Pb(II), Cu(II), Ni(II), Cd(II) ions onto polyethylene oxide or chitosan nanofiber membrane and at time limit of 0 to 400 min and it was noticed that 80 percent of the total amount of adsorbed metal ions took place in the first 60 min and attained equilibrium after 120 min. This result is of paramount importance since prolonged contact time can imbibe energy and, thereafter, inflate the remedy price.

4.2.3. Effect of initial concentration

The influence of initial adsorbate concentration is of importance in adsorption investigation because it is controlled by different variables including the nature of adsorbate and the liquid medium, the occurrence of competing cations, the presence of the adsorbent functional groups on the surface and the capability of these functional groups to bind adsorbate. Figs. 5a–c explain the plot. It was noticed in these figures that at a lower initial concentration of 0.5 mmol/L, the removal efficiency was high, but as the concentration rises to 2.5 mmol/L, the removal efficiency reduced; at rising concentration of adsorbate, the removal efficiency reduces owning to filling of the adsorbent surface/competition for a restricted number of unoccupied sites, which causes the adsorption site to be blocked. Also, at low concentrations, unoccupied sites are present and active for adsorbate adsorption [2]. Various investigations have published the influence of initial adsorbate concentration as a factor contributing to the binding of adsorbate onto different adsorbents and a number of them came up with comparable information from the present investigation study. [24] studied the adsorption of nickel on montmorillonite and noticed that the adsorption capacity raised with rising adsorbate concentration and after a marked concentration, a plateau was observed.
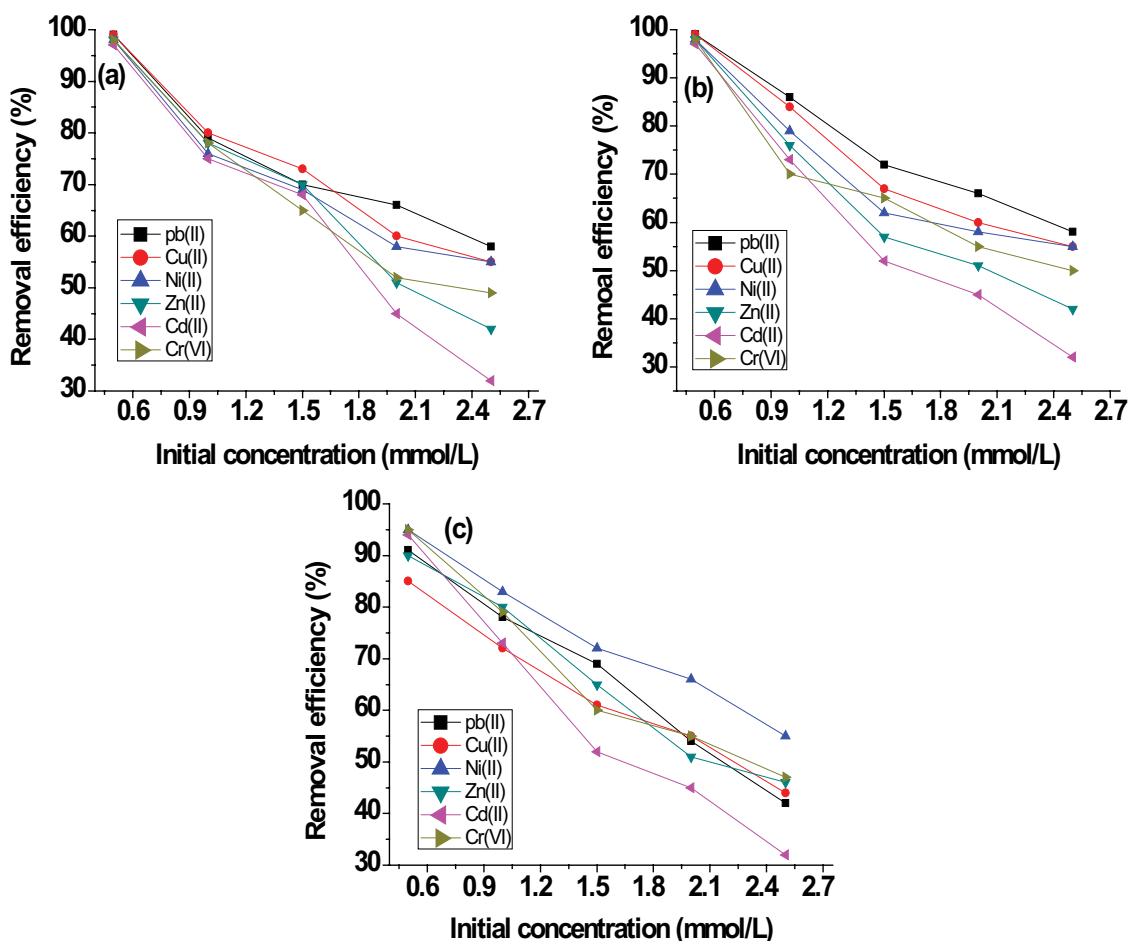
Fig. 5. Influence of initial concentration on percentage removal of adsorbate by (a) GXCS$_1$, (b) GXCS$_2$, and (c) GXCS$_3$, respectively (Conditions: pH: Pb^{2+}(5), Cd^{2+}(6), Zn^{2+}(6), Ni^{2+}(7), Cu^{2+}(5), and Cr^{6+}(6), contact time: 40 min, agitation speed: 120 rpm, and temperature: 45°C).

4.2.4. Effect of adsorbent dose

Figs. 6a–c describe the influence of adsorbent dose on the removal efficiency of metal ions. An obvious rise in removal efficiency of metal ions at the GXCS$_1$ dose range of 2–4 g was observed and an additional increase in dose did not result in any significant change. Also, a sharp increase was noticed for GXCS$_2$ and GXCS$_3$ at a dose range of 2–6 g and no additional increase in removal efficiency was recorded after 6 g. This observation at first is due to the presence of abundant binding sites for the adsorption of metal ions and increasing the dose beyond maximum limit resulted in the establishment of equilibrium between the metal ions bonded to GXCS$_1$, GXCS$_2$, and GXCS$_3$ respectively, and those remaining un-absorbed in the mixture [25]. A similar trend has been reported by [26], in their study on the binding of Pb^{2+} on palm kernel fiber. The increased percentage adsorption of these adsorbates with rising Tripolyphosphate–Kaolinite clay dose could be due to an increased surface negative charge and a decrease in the electrostatic potential near the solid surface that favors sorbent–solute interaction. The workers again reported that the rise in adsorbent dose at constant adsorbate concentration and volume will lead to the non-filling of binding sites via the adsorption process.

4.2.5. Effect of agitation speed

Figs. 7a–c describes the influence of agitation speed on removal efficiency of adsorbates by GXCS$_1$, GXCS$_2$, and GXCS$_3$ at agitation speed limit of 50–250 rpm. It was noticed that agitation speed has a positive influence on the removal of adsorbate by GXCS$_1$, GXCS$_2$, and GXCS$_3$. Also, there was a rise in the removal of adsorbate as the agitation speed is raised to 150 rpm and, thereafter, no significant changes were observed. A similar finding was reported by [27], who examined the influence of agitation speed on the binding of nickel onto natural zeolite and discovered that adsorption increased up until 150 rpm and then remained the same. Under high agitation speed, the external diffusion coefficient increases [28]. In most cases, the increase in stirring speed is associated with an increase in the rate of adsorption, particularly during the early stages of the process.

4.2.6. Effect of ionic strength

Figs. 8a–c explain the influence of ionic strength on the binding of Pb(II), Cu(II), Ni(II), Zn(II), Cd(II) and Cr(VI) ions onto GXCS$_1$, GXCS$_2$, and GXCS$_3$ respectively. In Fig. 8a, there was a minimal reduction in removal efficiency with a rising
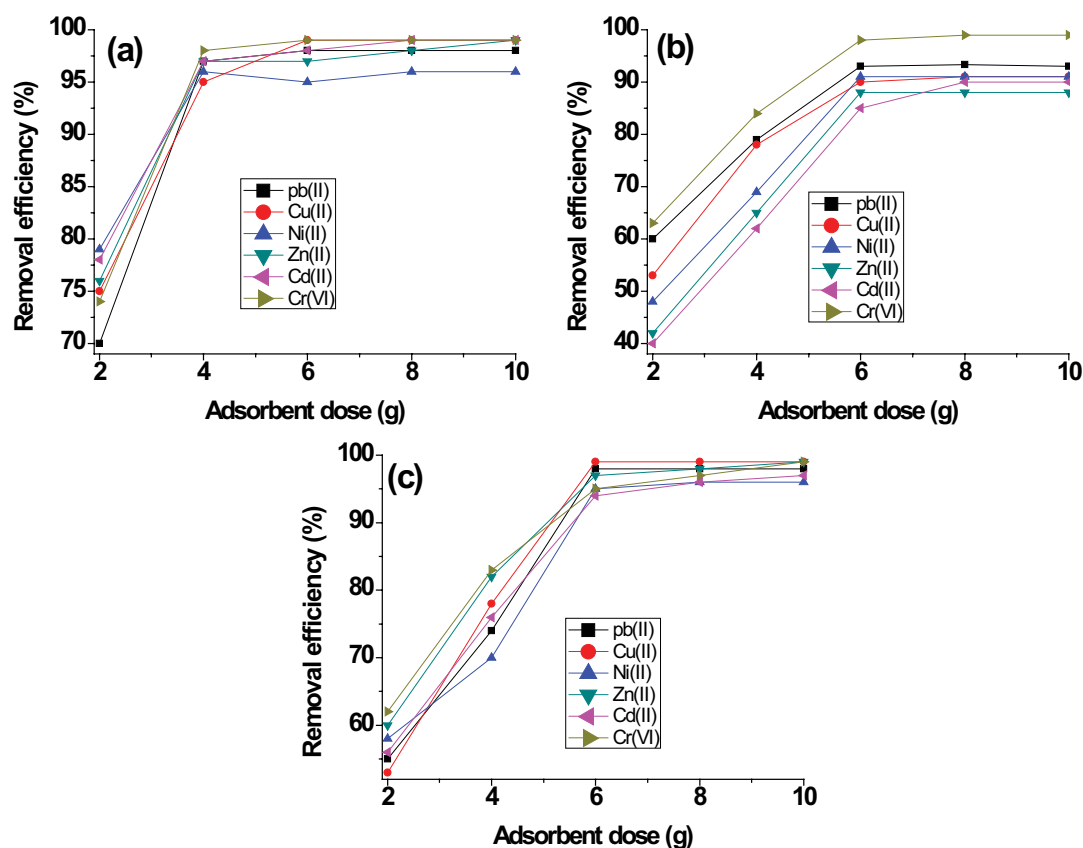
Fig. 6. Influence of (a) GXCS$_1$, (b) GXCS$_2$, and (c) GXCS$_3$ dose on percentage removal of adsorbate (Conditions: pH: Pb^{2+}(5), Cd^{2+}(6), Zn^{2+}(6), Ni^{2+}(7), Cu^{2+}(5), and Cr^{6+}(6), contact time: 40 min, initial concentration: 0.5 mmol/L, agitation speed: 120 rpm, and temperature: 45°C).

concentration of NaNO$_3$ in contrast to Figs. 8b and c. The cause of the decline in removal efficiency with rising ionic strength in these figures can be elucidated with regards to two points, first, movement of adsorbate to the adsorbent surface is not enough owing to the negative influence of ionic strength on the activity coefficient of the adsorbate. Secondly, from the theory of surface chemistry, when different waste such as waste from the industry and metal ions are in contact in an aqueous mixture, both are bound by an electrical double layer due to the electrostatic reaction which causes a decline in adsorption [2]. A similar result was presented by [29] on the influence of NaNO$_3$ at a concentration limit of 0.01–0.2 mol/L. Based on their study, the removal efficiency of Cu(II), Ni(II) and Pb(II) onto chitosan immobilized on bentonite was seen to be reducing with rising concentration of NaNO$_3$. The facts behind this remark, as stated by the authors, was due to the existence of Na$^+$ enclosing the outer layer of adsorbent upon the inclusion of NaNO$_3$ and a high NaNO$_3$ concentration specifies more Na$^+$ ions exist in the outer layer, which will utilize a high repelling force that repels the moving adsorbate, resulting in a reduction in removal efficiency.

4.3. Equilibrium parameters from pH model

The pH-model was used to describe the experimental results of equilibrium data of adsorbate binding onto GXCS$_1$,

GXCS$_2$, and GXCS$_3$, respectively. This demands the plotting of the left-hand side of Eq. (14) against pH at equilibrium. The acquired q_{max} for the respective adsorbent is presented in Table 1 and the values were found to be comparable to the total amine concentration calculated from the titration results; this shows that the amine groups are responsible for metal ions adsorption. The values of m and K_{ads} were obtained from the slope and intercept of Fig. 9 and are also given in Table 1. The number of amine groups and hydroxide groups that were involved in the metal adsorption were both found to be approximately one for these adsorbents. Consequently, the amine concentration of CS and XCS obtained from titration experiment was found to be 3.9 and 3.2 mmol/g respectively, while the amine concentration of the grafted beads was observed to be of higher value due to grafting reaction (Table 1). The DCL as calculated using Eq. (1) was found to be 17.9%.

4.4. Kinetic parameters

Tables 2 provides the values of the parameters of kinetic models applied for the binding of metal ions in batch mode onto GXCS$_1$, GXCS$_2$, and GXCS$_3$ respectively. Consequently, for the adsorption of metal ions onto ethylene acrylic acid grafted onto chitosan/glutaraldehyde composite GXCS$_1$, it is confirmed from the results (in Table 2) that the R^2 value
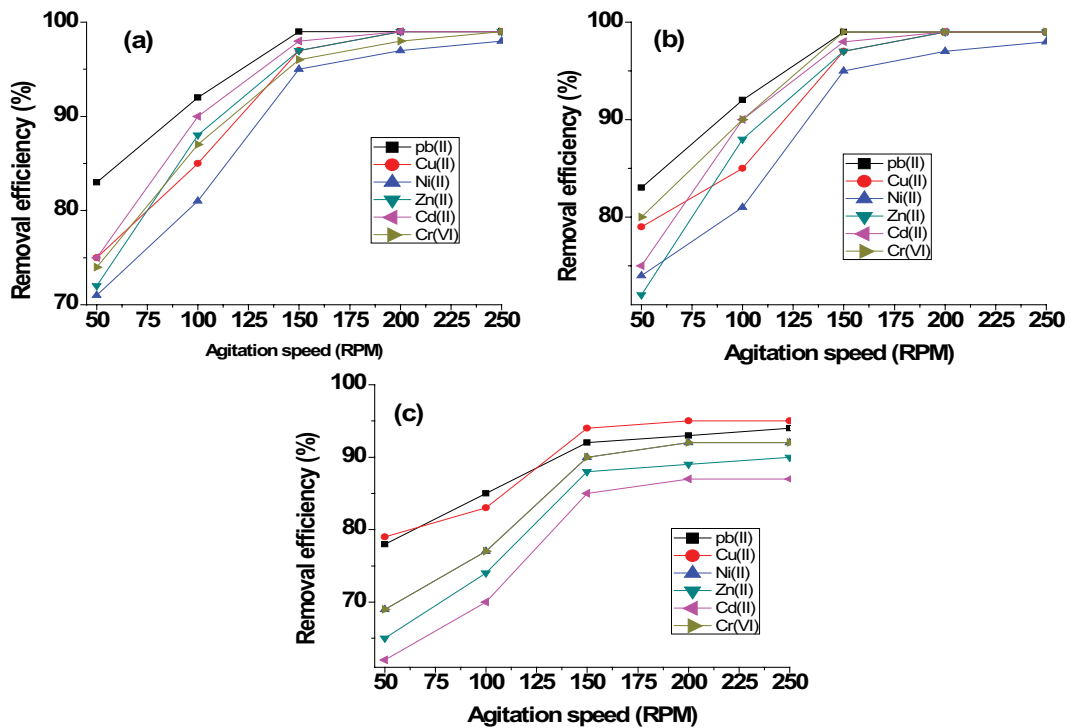
Fig. 7. Influence of agitation speed on percentage removal of adsorbate by (a) GXCS$_1$, (b) GXCS$_2$, and (c) GXCS$_3$, respectively (Conditions: pH: Pb^{2+}(5), Cd^{2+}(6), Zn^{2+}(6), Ni^{2+}(7), Cu^{2+}(5), and Cr^{6+}(6), contact time: 40 min, initial concentration: 0.5 mmol/L, and temperature: 45°C).
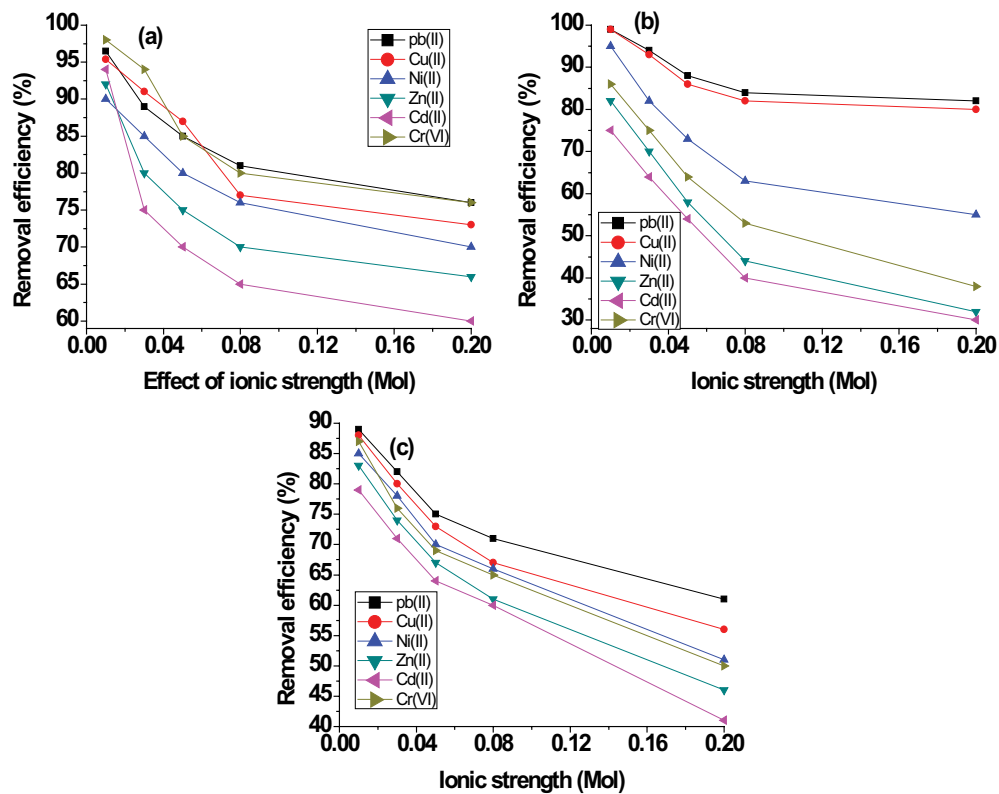

Fig. 8. Influence of ionic strength on percentage removal of adsorbate by (a) GXCS$_1$, (b) GXCS$_2$, and (c) GXCS$_3$, respectively (Conditions: pH: Pb^{2+}(5), Cd^{2+}(6), Zn^{2+}(6), Ni^{2+}(7), Cu^{2+}(5), and Cr^{6+}(6) contact time: 40 min, initial concentration: 0.5 mmol/L, and temperature: 45°C).
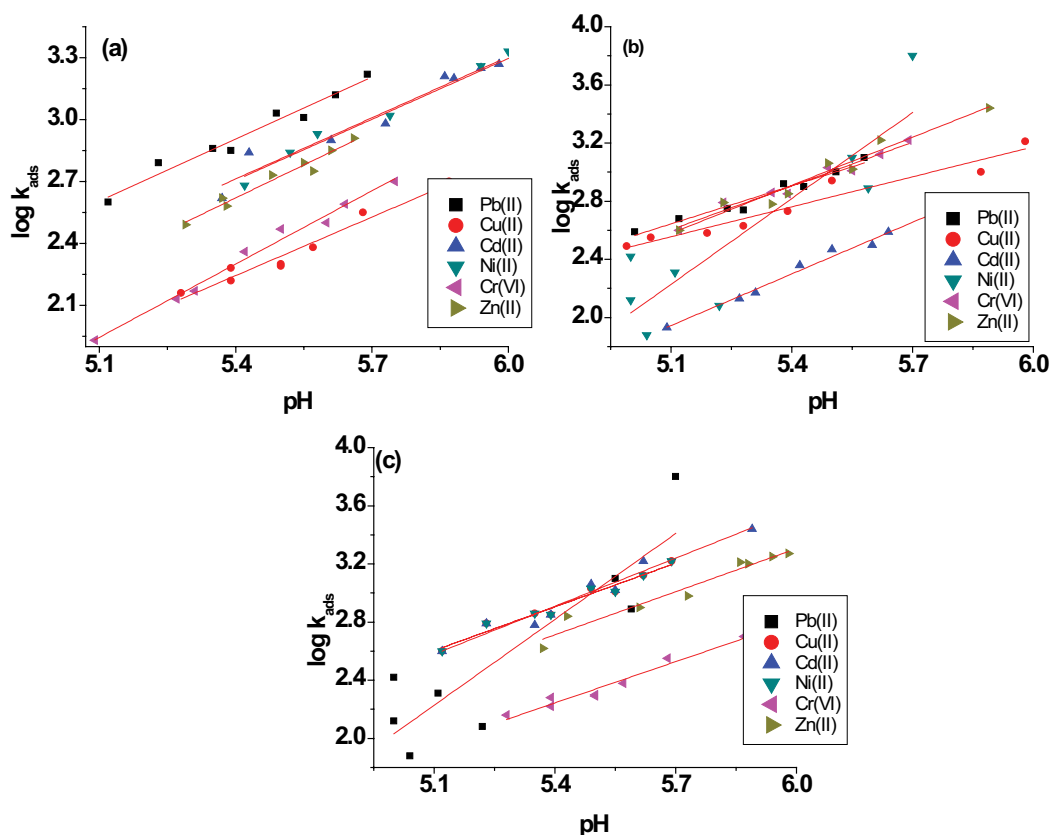
Fig. 9. Equilibrium constant measurements for metal ions adsorption onto modified bead by (a) $GXCS_1$, (b) $GXCS_2$, and (c) $GXCS_3$.

Table 1
Equilibrium parameters for metal ions adsorption onto by $GXCS_1$, $GXCS_2$, and $GXCS_3$, respectively

Adsorbent	Metal ions	m	K_{ads} (1.0×10^{-4})	q_{max} (mmol/g)	(−NH$_2$) (mmol/g)	R^2
GXC_S1	Pb(II)	1.0	9.5	4.8	5.60	0.949
	Cu(II)	1.0	2.5	4.8	5.60	0.982
	Ni(II)	0.9	2.9	4.8	5.60	0.965
	Cd(II)	1.2	4.1	4.8	5.60	0.958
	Cr(VI)	1.1	3.1	4.8	5.60	0.976
	Zn(II)	1.0	2.6	4.8	5.60	0.923
$GXCS_2$	Pb(II)	0.9	1.8	4.4	5.30	0.941
	Cu(II)	1.2	4.1	4.4	5.30	0.960
	Ni(II)	1.0	7.8	4.4	5.30	0.987
	Cd(II)	1.1	2.5	4.4	5.30	0.943
	Cr(VI)	1.1	3.0	4.4	5.30	0.965
	Zn(II)	0.8	2.5	4.4	5.30	0.956
$GXCS_3$	Pb(II)	0.9	7.8	4.0	4.70	0.960
	Cu(II)	0.9	5.7	4.0	4.70	0.987
	Ni(II)	1.1	9.3	4.0	4.70	0.943
	Cd(II)	1.2	4.4	4.0	4.70	0.965
	Cr(VI)	0.8	4.8	4.0	4.70	0.950
	Zn(II)	0.9	2.6	4.0	4.70	0.986

Table 2
Kinetic parameters for the binding of considered metal ions onto $GXCS_1$ at pH of Pb(5), Cd(6), Zn(6), Ni(7), Cu(5), and Cr(6), respectively, temperature of 45°C, stirring speed of 150 RPM and contact time of 40 min

Metal ions	Pseudo-first-order parameters				Experimental values	Pseudo-second-order parameters				Intra-particle diffusion parameters	
	K_1 (min^{-1})	$q_{e,\text{pred}}$ (mmol/g)	MPSD	R^2	$q_{e,\text{exp}}$ (mmol/g)	K_2 (g/mmol min)	$q_{e,\text{pred}}$ (mmol/g)	MPSD	R^2	K_{idm} (mmol/gmin$^{1/2}$)	R^2
Pb(II)	0.011	1.93 ± 0.01	33.861	0.842	4.36 ± 0.05	7.785	4.38 ± 0.04	1.242	0.999	7.103	0.999
Cu(II)	0.024	1.98 ± 0.02	30.212	0.799	4.79 ± 0.03	8.223	4.78 ± 0.05	2.314	0.999	7.595	0.973
Ni(II)	0.021	1.95 ± 0.02	14.305	0.821	3.33 ± 0.01	6.167	3.35 ± 0.02	0.985	0.999	7.131	0.962
Cr(VI)	0.045	2.10 ± 0.01	9.313	0.793	3.19 ± 0.02	5.942	3.22 ± 0.02	4.121	0.999	6.164	0.996
Zn(II)	0.012	1.75 ± 0.01	15.391	0.885	3.14 ± 0.01	4.598	3.11 ± 0.01	4.226	0.999	5.323	0.975
Cd(II)	0.031	2.14 ± 0.02	8.432	0.793	2.58 ± 0.01	4.321	2.54 ± 0.01	4.982	0.986	4.987	0.988

Table 3
Kinetic parameters for the binding of considered metal ions onto $GXCS_2$ at pH of Pb(5), Cd(6), Zn(6), Ni(7), Cu(5), and Cr(6), respectively, temperature of 45°C, stirring speed of 150 RPM and contact time of 60 min

Metal ions	Pseudo-first-order parameters				Experimental values	Pseudo-second-order parameters				Intra-particle diffusion parameters	
	K_1 (min^{-1})	$q_{e,\text{pred}}$ (mmol/g)	MPSD	R^2	$q_{e,\text{exp}}$ (mmol/g)	K_2 (g/mmol min)	$q_{e,\text{pred}}$ (mmol/g)	MPSD	R^2	K_{idm} (mmol/gmin$^{1/2}$)	R^2
Pb(II)	0.033	1.59 ± 0.01	34.212	0.882	3.42 ± 0.07	7.342	3.54 ± 0.06	1.442	0.983	3.432	0.979
Cu(II)	0.016	1.16 ± 0.01	31.672	0.813	3.81 ± 0.09	5.285	3.87 ± 0.04	3.983	0.999	4.185	0.994
Ni(II)	0.022	1.90 ± 0.03	16.274	0.831	3.19 ± 0.06	5.121	3.12 ± 0.07	2.872	1.000	2.976	0.996
Cr(VI)	0.032	2.20 ± 0.08	12.127	0.836	3.80 ± 0.04	3.213	3.99 ± 0.05	6.327	0.999	2.565	0.983
Zn(II)	0.021	1.67 ± 0.02	16.521	0.873	3.59 ± 0.06	4.743	3.53 ± 0.04	3.128	0.987	3.163	0.999
Cd(II)	0.055	1.85 ± 0.01	8.978	0.732	3.45 ± 0.05	2.561	2.52 ± 0.02	3.443	0.999	3.784	0.999

Table 4
Kinetic parameters for the binding of considered metal ions onto $GXCS_3$ at pH of Pb(5), Cd(6), Zn(6), Ni(7), Cu(5), and Cr(6), respectively, temperature of 45°C, stirring speed of 150 RPM and contact time of 60 min

Metal ions	Pseudo-first-order parameters				Experimental values	Pseudo-second-order parameters				Intra-particle diffusion parameters	
	K_1 (min^{-1})	$q_{e,\text{pred}}$ (mmol/g)	MPSD	R^2	$q_{e,\text{exp}}$ (mmol/g)	K_2 (g/mmol min)	$q_{e,\text{pred}}$ (mmol/g)	MPSD	R^2	K_{idm} (mmol/gmin$^{1/2}$)	R^2
Pb(II)	0.012	1.32 ± 0.01	35.552	0.831	2.81 ± 0.01	8.521	2.89 ± 0.01	2.162	0.962	7.653	0.999
Cu(II)	0.033	1.36 ± 0.02	31.231	0.762	3.10 ± 0.03	7.872	3.14 ± 0.02	4.324	0.991	7.894	0.943
Ni(II)	0.082	1.28 ± 0.02	12.324	0.861	3.00 ± 0.02	7.434	2.98 ± 0.04	2.323	0.974	5.871	0.972
Cr(VI)	0.014	1.02 ± 0.01	8.123	0.784	2.42 ± 0.01	4.313	2.47 ± 0.02	3.984	0.993	3.672	0.954
Zn(II)	0.041	1.22 ± 0.01	16.561	0.871	5.59 ± 0.06	5.683	2.86 ± 0.01	3.783	0.962	4.231	0.932
Cd(II)	0.092	0.76 ± 0.01	6.651	0.792	4.71 ± 0.03	4.542	2.50 ± 0.01	6.172	0.952	3.904	0.981

for the pseudo-second-order and intra-particle model are stronger and nearer to one in contrast to pseudo-first-order model. The experimental q_e values derived from the pseudo-second-order were inconsistent with the predicted q_e, while the experimental q_e values from the pseudo-first-order were not consistent with the predicted q_e. However, the small Marquardt's percent standard deviation (MPSD) values, which are in the range of 0.985 to 4.982 from the pseudo-second-order model denote remarkable consistency to experimental and predicted data, whereas the high MPSD values, which were found to be in the limit of 8.432 to 33.861 from the pseudo-first-order model represent a deficient agreement to experimental and predicted data. This technique of examining experimental data again demonstrates the suitability of the pseudo-second-order model. A similar report was presented by [16]. Consequently, the same

Table 5
Desorption behavior of Pb(II), Cu(II), Ni(II), Cd(II), Cr(VI), and Zn(II) ions onto GXCS$_1$, GXCS$_2$, and GXCS$_3$, respectively

Binding onto GXCS$_1$	% Desorption	q_{max} (mmol/g)
Pb(II)	99.10	4.79 ± 0.08
Cu(II)	99.30	4.80 ± 0.05
Ni(II)	97.60	4.78 ± 0.04
Cd(II)	98.00	4.70 ± 0.02
Cr(VI)	99.00	4.75 ± 0.01
Zn(II)	97.60	4.73 ± 0.01
Binding onto GXCS$_2$		
Pb(II)	98.80	4.37 ± 0.03
Cu(II)	97.50	4.39 ± 0.04
Ni(II)	97.90	4.36 ± 0.02
Cd(II)	97.70	4.36 ± 0.01
Cr(VI)	98.00	4.32 ± 0.02
Zn(II)	98.30	4.36 ± 0.02
Binding onto GXCS$_3$		
Pb(II)	97.80	4.00 ± 0.03
Cu(II)	98.30	3.98 ± 0.02
Ni(II)	99.60	3.97 ± 0.02
Cd(II)	98.20	3.97 ± 0.01
Cr(VI)	99.00	3.95 ± 0.02
Zn(II)	97.50	3.96 ± 0.01

observation was found for the other two sets of beads, that is, 4-aminobenzoic acid grafted onto chitosan/glutaraldehyde composite GXCS$_2$ and ethylenediaminetetraacetic acid grafted onto chitosan/glutaraldehyde composite GXCS$_3$, as presented in Tables 3 and 4, respectively.

4.5. Regeneration investigation

Adsorbent regeneration ensures a reduction in the cost of process operation and the retrieval of metal ions for acceptable discarding in an attempt to stop re-polluting the environment. During the process of regeneration, the used adsorbents were washed separately with distilled water before treating with 0.5 M HCl at a contact time of 180 min. After chemical treatment of the used beads, there was no loss in the weight of the adsorbent and the changes in the maximum adsorption capacity was negligible even up to the fourth cycle. Table 5 presents only the desorption behavior of the metal ions adsorption in the first cycle.

4.6. Conclusion

Three promising adsorbents were developed by separately grafting ethylene acrylic acid, 4-aminobenzoic acid, and ethylenediaminetetraacetic acid onto the backbone of cross-linked chitosan beads, which reduced its crystallinity and expanded the polymer network for easy accessibility of the considered metal ions to the binding site. A comprehensive investigation was performed on each adsorbent to access the effect adsorption parameters have on the binding of metal ions. The adsorption of Pb(II), Cu(II), Ni(II), Zn(II), Cd(II)

and Cr(VI) was dependent on pH, contact time, adsorbent dosage, initial concentration, and ionic strength. However, the pH equilibrium model was revealed to conveniently explain the adsorption of metal ions onto the modified beads. The model was obtained based on two equilibrium equations, one explaining the characteristics of the acid-base reaction of the modified bead and the second one explaining the binding of adsorbate onto the modified bead. The total amount of amine groups and hydroxide groups that took part in the metal adsorption was each found to be one for the three different prepared adsorbents. The binding of metal ions onto adsorbents was also observed to agree with pseudo-second-order and intra-particle diffusion kinetic models. These results indicated that the binding of metal ions onto GXCS$_1$, GXCS$_2$ and GXCS$_3$ were observed to be a complex operation comprising mainly of chelation, chemisorption, electrostatic attraction or ion exchange. The multi-functional group present in GXCS$_1$ was instrumental in the binding of metal ions even at a low pH value. Among the adsorbents considered in this study, GXCS$_1$ proved to be more effective by being able to adsorb more than half of each studied metal ions at a low pH of 2. The GXCS$_1$ adsorbent was able to establish equilibrium in 40 min in comparison to the later time of equilibrium of GXCS$_2$ and GXCS$_3$ respectively. At the industrial level, these formulated adsorbent materials can be an excellent candidate for the adsorption of adsorbates.

References

[1] H. Alijani, Z. Shariatinia, A. Aroujalian Mashhadi, Water assisted synthesis of MWCNTs over natural magnetic rock: an effective magnetic adsorbent with enhanced mercury(II) adsorption property, Chem. Eng. J., 281 (2015) 468–481.

[2] E. Igberase, P. Osifo, A. Ofomaja, Adsorption of metal ions by microwave assisted grafting of cross-linked chitosan beads. equilibrium, isotherm, thermodynamic and desorption studies, Appl. Organomet. Chem., 32 (2017), https://doi.org/10.1002/aoc.4131.

[3] D. Sud, G. Mahajan, M.P. Kaur, Agricultural waste material as potential adsorbent for sequestering heavy metal ions from aqueous solutions - a review, Bioresour. Technol., 99 (2008) 6017–6027.

[4] S. Malamis, E. Katsou, A review on zinc and nickel adsorption on natural and modified zeolite, bentonite and vermiculite: examination of process parameters, kinetics and isotherms, J. Hazard. Mater., 252–253 (2013) 428–461.

[5] P. Kampalanonwat, P. Supaphol, The study of competitive adsorption of heavy metal ions from aqueous solution by aminated polyacrylonitrile nanofiber mats, Energy Procedia, 56 (2014) 142–151.

[6] M. Madhava Rao, A. Ramesh, G. Purna Chandra Rao, K. Seshaiah, Removal of copper and cadmium from the aqueous solutions by activated carbon derived from *Ceiba pentandra* hulls, J. Hazard. Mater., 129 (2006) 123–129.

[7] E. Igberase, A. Ofomaja, P.O. Osifo, Enhanced heavy metal ions adsorption by 4-aminobenzoic acid grafted on chitosan/epichlorohydrin composite: kinetics, isotherms, thermodynamics and desorption studies, Int. J. Biol. Macromol., 123 (2019) 664–676.

[8] E. Igberase, P.O. Osifo, Mathematical modelling and simulation of packed bed column for the efficient adsorption of Cu(II) ions using modified bio-polymeric material, J. Environ. Chem. Eng., 7 (2019) 103129.

[9] E. Igberase, P.O. Osifo, Application of diethylenetriamine grafted on glyoxal cross-linked chitosan composite for the effective removal of metal ions in batch system, Int. J. Biol. Macromol., 134 (2019) 1145–1155.

[10] S. Chatterjee, I. Sivareddy, S. De, Adsorptive removal of potentially toxic metals (cadmium, copper, nickel and zinc) by chemically treated laterite: Single and multicomponent batch and column study, J. Environ. Chem. Eng., 5 (2017) 3273–3289.

[11] E. Igberase, P. Osifo, A. Ofomaja, Mathematical modelling of Pb^{2+}, Cu^{2+}, Ni^{2+}, Zn^{2+}, Cr^{6+} and Cd^{2+} ions adsorption from a synthetic acid mine drainage onto chitosan derivative in a packed bed column, Environ. Technol. (United Kingdom), 39 (2017) 3203–3220.

[12] P.O. Osifo, H.W.J.P. Neomagus, H. van der Merwe, D.J. Branken, Transport properties of chitosan membranes for zinc (II) removal from aqueous systems, Sep. Purif. Technol., 179 (2017) 428–437.

[13] P.O. Osifo, A. Webster, H. van der Merwe, H.W.J.P. Neomagus, M.A. van der Gun, D.M. Grant, The influence of the degree of cross-linking on the adsorption properties of chitosan beads, Bioresour. Technol., 99 (2008) 7377–7382.

[14] Y.S. Ho, G. McKay, Application of kinetic models to the sorption of copper(II) on to peat, Adsorpt. Sci. Technol., 20 (2002) 797–815.

[15] K.S. Hui, C.Y.H. Chao, S.C. Kot, Removal of mixed heavy metal ions in wastewater by zeolite 4A and residual products from recycled coal fly ash, J. Hazard. Mater., 127 (2005) 89–101.

[16] A. Itodo, F. Abdulrahman, L. Hassan, S.A. Maigandi, H. Itodo, Intraparticle diffusion and intraparticulate diffusivities of herbicide on derived activated carbon, Researcher, 2 (2010) 74–86.

[17] V.N. Tirtom, A. Dinçer, S. Becerik, T. Aydemir, A. Çelik, Comparative adsorption of Ni(II) and Cd(II) ions on epichlorohydrin crosslinked chitosan-clay composite beads in aqueous solution, Chem. Eng. J., 197 (2012) 379–386.

[18] Z. Wei, Y. Luo, B. Li, Z. Cheng, J. Wang, Q. Ye, Microwave assisted catalytic removal of elemental mercury from flue gas using Mn/zeolite catalyst, Atmos. Pollut. Res., 6 (2015) 45–51.

[19] L. Zhang, Y. Zeng, Z. Cheng, Removal of heavy metal ions using chitosan and modified chitosan: a review, J. Mol. Liq., 214 (2016) 175–191.

[20] S. Nagireddi, V. Katiyar, R. Uppaluri, Pd(II) adsorption characteristics of glutaraldehyde cross-linked chitosan copolymer resin, Int. J. Biol. Macromol., 94 (2017) 72–84.

[21] E. Igberase, P. Osifo, Equilibrium, kinetic, thermodynamic and desorption studies of cadmium and lead by polyaniline grafted cross-linked chitosan beads from aqueous solution, J. Ind. Eng. Chem., 26 (2015) 340–347.

[22] A.A. Taha, M.A. Shreadah, A.M. Ahmed, H.F. Heiba, Multi-component adsorption of Pb(II), Cd(II), and Ni(II) onto Egyptian Na-activated bentonite; equilibrium, kinetics, thermodynamics, and application for seawater desalination, J. Environ. Chem. Eng., 4 (2016) 1166–1180.

[23] M. Aliabadi, M. Irani, J. Ismaeili, H. Piri, M.J. Parnian, Electrospun nanofiber membrane of PEO/Chitosan for the adsorption of nickel, cadmium, lead and copper ions from aqueous solution, Chem. Eng. J., 220 (2013) 237–243.

[24] C.O. Ijagbemi, M.H. Baek, D.S. Kim, Montmorillonite surface properties and sorption characteristics for heavy metal removal from aqueous solutions, J. Hazard. Mater., 166 (2009) 538–546.

[25] C. Dong, F. Zhang, Z. Pang, G. Yang, Efficient and selective adsorption of multi-metal ions using sulfonated cellulose as adsorbent, Carbohydr. Polym., 151 (2016) 230–236.

[26] Y.S. Ho, A.E. Ofomaja, Kinetics and thermodynamics of lead ion sorption on palm kernel fibre from aqueous solution, Process Biochem., 40 (2005) 3455–3461.

[27] S. Kocaoba, Y. Orhan, Kinetics and equilibrium studies of heavy metal ions removal by use of natural zeolite, Desalination, 214 (2007) 1–10.

[28] J. Shen, Z. Duvnjak, Adsorption kinetics of cupric and cadmium ions on corncob particles, Process Biochem., 40 (2005) 3446–3454.

[29] C.M. Futalan, C.C. Kan, M.L. Dalida, K.J. Hsien, C. Pascua, M.W. Wan, Comparative and competitive adsorption of copper, lead, and nickel using chitosan immobilized on bentonite, Carbohydr. Polym., 83 (2011) 528–536.